Anal. Chem. **1997,** *69,* 2871−2876

Articles

Multielemental Chemical Imaging Using Laser-Induced Breakdown Spectrometry

Dolores Romero and J. Javier Laserna*

Department of Analytical Chemistry, Faculty of Sciences, University of Málaga, E29071 Málaga, Spain

Multichannel laser-induced breakdown spectrometry (LIBS) is used to generate selective chemical images for silver, titanium, and carbon from silicon photovoltaic cells. A 2.5 mJ pulsed nitrogen laser and a spectrometer using charge-coupled device detection were employed. LIBS images were acquired sequentially by moving the sample located on a motorized *x*−*y* translational stage step by step while storing the multichannel LIBS spectrum for each position of the sample, followed by computer-based reconstruction of two-dimensional selective images from intensity profiles at several wavelengths. Depth distributions of carbon impurities are also reported. Room temperature and atmospheric pressure operation as used here remove the restrictions on sample size exhibited by other surface analysis techniques used for imaging applications. Thus, the sample size in LIBS imaging is in principle unlimited. A LIBS experiment does not require a sample to be conductive. Therefore, virtually all materials can be imaged. Although LIBS is a typical example of destructive analytical technique, multichannel detection as demonstrated here confers the possibility to LIBS of obtaining multielement information from a given surface area. Lateral resolution of 80 μm and depth resolution of better than 13 nm were observed. The ultimate limitation to imaging the first layer of the surface in LIBS is the spectral signal-to-noise ratio as dictated by the ablation threshold of the material.

Significant progress in chemical information from bulk analysis to spatially resolved analysis has occurred in the last decade. Many subjects of key interest in science and technology require a knowledge of local distribution and concentration gradients rather than averaged concentrations as provided by bulk analysis methods. The term chemical imaging has been coined to describe the information provided by some classes of imaging methods. Many forms of imaging provide topographic details from the sample under study. However, production of chemical images is restricted to those methods that can incorporate information on chemical identity to spatial dimensions. The term chemical image thus refers to the spatial distribution of single chemical species within a multicomponent sample. Although the term image could be also applied to monodimensional information such as depth profiles or lateral cross sections, chemical imaging refers more properly to the production of chemical information in 2-D or higher dimensionality formats. Advancement in this area has resulted in the development of a number of methods capable of producing analytical data in image form. They include the use of radio frequency (magnetic resonance imaging), infrared, visible, and ultraviolet photons (remote sensing, Raman imaging, fluorescence, confocal microscopy), X-rays (X-ray tomography, X-ray microfluorescence, X-ray photoelectron spectroscopy), electrons (scanning and transmission electron microscopies, electron energy loss spectrometry, scanning Auger electron spectroscopy, scanning tunneling microscopy, atomic force microscopy), ions (secondary ion mass spectroscopy, particle-induced X-ray emission), and protons (Rutherford backscattering spectroscopy). A number of reviews on chemical imaging are available.[1−5]

Laser-induced breakdown spectroscopy (LIBS) has been applied for analytical purposes since 1962.[6] In general, a pulsed laser is required as only high-energy pulses focused to a small spot produce enough irradiance to reach the ablation threshold of solid materials. Earlier instruments incorporated additional excitation of the laser plasma with a crossed spark in order to increase the spectral emission and to reduce the effect on precision of shot-to-shot laser variability. Although this approach fostered the detection power of LIBS, spark excitation was soon eliminated

(1) Van Espen, P.; Janssens, G.; Vanhoolst, W.; Geladi, P. *Analusis* **1992**, *20*, 81−90.
(2) Bertrand, D.; Devaux, M. F.; Robert, P. *Trends Anal. Chem.* **1991**, *10*, 237−243.
(3) Geladi, P.; Bengtsson, E.; Esbensen, K.; Grahn, H. *Trends Anal. Chem.* **1992**, *11*, 41−53.
(4) Geladi, P.; Grahn, H.; Esbensen, K.; Bengtsson, E. *Trends Anal. Chem.* **1992**, *11*, 121−130.
(5) Grasserbauer, M. *Fresenius Z. Anal. Chem.* **1985**, *322*, 105−123.
(6) Brech, F. *Appl. Spectrosc.* **1962**, *16*, 59.

S0003-2700(97)00311-9 CCC: $14.00

when lasers with improved beam quality and stabilized energy output were available. LIBS has been recently applied to the analysis of solids,[7−9] liquids,[10] gases,[11] and aerosols.[12] The analytical applications of LIBS have been discussed in a number of reviews[13,14] and book chapters.[15−18]

As early as in 1968, Adams and Tong suggested the use of lasers to map the distribution of atomic species on surfaces.[19] A ruby laser microscope was used as a sampling method to volatilize a chosen area in the surface. The vaporized material was condensed on a transparent cover plate and analyzed by radiometric methods and mass spectrometry. This approach was applied to UO_2 pellets from nuclear fuels, but no further surface information was provided. Local analysis based on optical emission spectrometry of laser-produced plasmas has been thoroughly reviewed by Moenke-Blankenburg.[18] Lateral profiles of solid surfaces using LIBS were demonstrated for Mo impurities across a blemish on a ceramic tube.[20] The capabilities of LIBS for depth profiling have been discussed.[21] Zn/Ni, Sn, and Cr coatings on steel were detected with good precision. Recently, the use of LIBS for monitoring the thickness of TiO_2 coatings was reported.[22]

Thus, while the idea of LIBS imaging has been around for some time, the technique has been demonstrated just recently.[23] The analysis of coating coverage, coat weight distribution, and 3-D distribution of Ca and Si of paper coatings were described. Using a photomultiplier-based monochannel instrument, single-element information of a given surface area was obtained. Since LIBS is destructive, no additional element information from a given area can be obtained.

In this paper, multielement LIBS imaging is demonstrated. Incorporation of a multichannel detector to the spectrometric system confers the possibility to LIBS of obtaining multielemental imaging information in a single data acquisition routine. Thus, apart from geometric dimensions, LIBS images are also multidimensional in the spectroscopic sense, each image representing the spatial distribution of a particular atomic species. This multidimensionality is essential and typical of the LIBS method of producing chemical images. In this paper, the imaging capabilities of multichannel LIBS are demonstrated using silicon photovoltaic cells as model substrates.

EXPERIMENTAL SECTION

The experimental set up consisted of a pulsed nitrogen laser (Laser Photonics model UV-12, wavelength 337.1 nm, pulse width 10 ns, nominal pulse energy 2.5 mJ) focused on solid samples at normal incidence at room temperature, in air at 760 Torr, using a planoconvex quartz lens with a focal length of 45 mm and *f* 0.5. Samples were placed in a vertical fashion. Laser plasma emission was collected with a biconvex quartz lens with a focal length of 55 mm onto the entrance slit of a triple indexable Czerny-Turner grating spectrograph (Acton Research Corp., Model Spectra Pro 275, focal length 275 mm) fitted with classically ruled gratings of 300, 600, and 1200 grooves/mm blazed at 600 nm. The reciprocal linear dispersion of the spectrograph was 12 nm/mm with the 300 grooves/mm grating, giving a spectral coverage of 116.4 nm for the detector used. The spectrograph entrance slit was 15 mm high and 20 μm wide. The plasma axis was perpendicular to the spectrograph entrance slit. The plasma-dispersed light was detected with a solid-state two-dimensional charge-coupled device (CCD; EG&G PAR, Thomson CSF, Model THX-31159A) cooled to −60 °C by a Peltier system. The CCD consists of 512 × 512 pixels, each 19 μm × 19 μm. The active area is 9.7 mm × 9.7 mm. This CCD system has a quantum efficiency of 27% at 500 nm. When cooled to −60 °C, this detector exhibits a dark current of 10 photoelectrons pixel^{-1} s^{-1} and spectral response in the range 400−900 nm. Calibration of the detector system is conducted with a mercury pen lamp. For data acquisition, the CCD system was optically triggered with a beam deflected from the laser beam and a fast photodiode. The dispersed image of the plasma was then integrated using an acquisition time of 100 ms and binned in the vertical direction to produce a single spectrum. Operation of the detector was controlled by a personal computer with OMA Spec 4000 software. Samples were placed on two crossed translational motorized stages (Physik Instrumente) controlled by computer, which allow an exact stepwise movement of the sample in both directions *x* and *y* at minimum increments of 10 μm. Laser trigger was controlled externally by a digital delay/pulse generator (Stanford Research System Model DG535). A laboratory-developed software written in Turbo C^{++} language allows the exact synchronization between the translational stage movement and the laser firing. Communication between devices was carried out by an IEEE 488 general purpose interface bus (GPIB) interface. Data reduction was accomplished in a standard personal computer with commercial software. Silicon photovoltaic cells were provided by Isofotón S. A. (Málaga, Spain). Photovoltaic cells are 3-D structures formed by textured silicon wafers covered by a 40-nm epitaxial layer of TiO_2. A periodic array of silver fingers produced by lithography is then marked on the cell surface to collect charge from the p−n junction in the Si wafer. Prior to TiO_2 deposition, silicon wafers were textured in order to decrease their reflectivity. Textured surfaces were produced by anisotropic etching of silicon with dilute NaOH solutions. The appearance of the textured silicon surface is an array of square-based pyramids formed by the intersection of the (111) crystal planes.

RESULTS AND DISCUSSION

The fact that micrometer-sized surface areas can be analyzed and that the sample can be moved systematically make LIBS an

(7) Thiem, T. L.; Salter, R. H.; Gardner, J. A.; Lee, Y. I.; Sneddon, J. *Appl. Spectrosc.* **1994**, *48*, 58−63.
(8) Eppler, A. S.; Cremers, D. A.; Hickmott, D. D.; Ferris, M. J.; Koskelo, A. C. *Appl. Spectros.* **1996**, *50*, 1175−1181.
(9) Nemet, B.; Kozma, L. *Spectrochim. Acta* **1995**, *50*, 1869−1888.
(10) Knopp, R.; Scherbaun, F. J.; Kim, J. I. *Fresenius J. Anal. Chem.* **1996**, *355*, 16−20.
(11) Singh, J. P.; Zhang, H.; Yueh, F-Y.; Carney, K. P. *Appl. Spectrosc.* **1996**, *50*, 764−773.
(12) Radziemski, L. J.; Loree, T. R.; Cremers, D. A.; Hoffman, N. M. *Anal. Chem.* **1983**, *55*, 1246−1252.
(13) Majidi,V.; Joseph, M. R. *Crit. Rev. Anal. Chem.* **1992**, *23*, 143−162.
(14) Radziemsky, L. J. *Microchem. J.* **1994**, *50*, 218−234.
(15) Radziemsky, J. L.; Cremers, D. A. In *Laser-Induced Plasmas and Applications*; Radziemsky, J. L., Cremers, D. A., Eds.; Marcel Dekker: New York, 1989, pp 295−325.
(16) Kim, Y. W. In *Laser-Induced Plasmas and Applications*; Radziemsky, J. L., Cremers, D. A., Eds.; Marcel Dekker: New York, 1989; pp 327−346.
(17) Piepmeier, E. H. In *Analytical Applications of Lasers*; Piepmeier, E. H., Ed.; Wiley: New York, 1986; pp 627−669.
(18) Moenke-Blankenburg, L. *Laser Microanalysis*; Wiley: New York, 1989; pp 93−180.
(19) Adams, M. D.; Tong, S. C. *Anal. Chem.* **1968**, *40*, 1762−1765.
(20) Talmi, Y.; Sieper, H. P.; Moenke-Blankenburg, L. *Anal. Chim. Acta* **1981**, *127*, 71−85.
(21) Anderson, D. R.; McLeod, C. W.; English, T.; Smith, A. T. *Appl. Spectrosc.* **1995**, *49*, 691−701.
(22) Hidalgo, M:; Martín, F.; Laserna, J. J. *Anal. Chem.* **1996**, *68*, 1095−1100.
(23) Häkkänen, H. J.; Korppi-Tommola, J. E. I. *Appl. Spectrosc.* **1995**, *49*, 1721−1728.

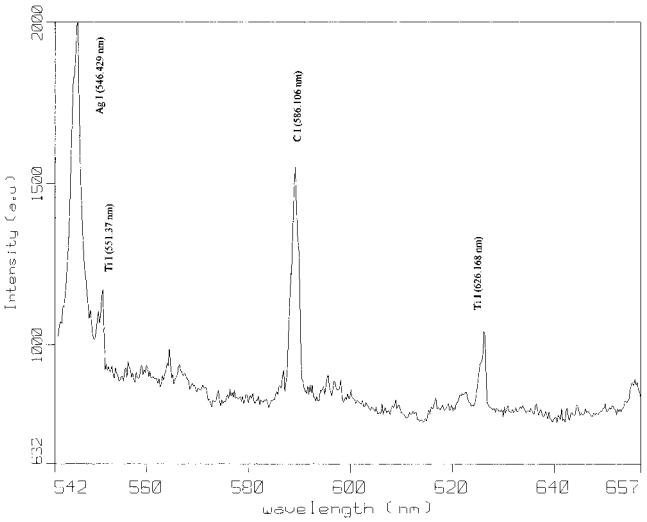

Figure 1. Single-shot LIBS spectrum from a silicon photovoltaic cell surface in a zone located in the interphase between a silver finger and the Ti coating showing the most relevant emission lines from a silicon photovoltaic cell. Laser irradiance 1.7×10^8 W cm^{-2}.

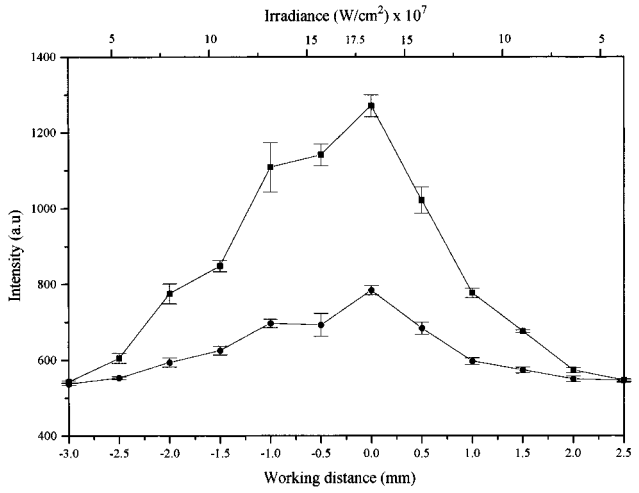

Figure 2. Spectral line intensity of (■) titanium I 626.128 nm and (●) background measured at 627.3 nm as function of the working distance and laser irradiance. Bars correspond to the range of five measurements.

ideal mapping tool. LIBS images show optical emission intensities as a function of location on sample surfaces. A static finely focused laser beam impinges on the sample. If the laser irradiance at the surface is larger than the ablation threshold of the sample material, a laser plasma is formed. The spectral emission is then collected using the transfer optics to the spectrometer entrance slit. Two-dimensional images are acquired sequentially by moving the sample located on a $x-y$ translational stage step by step while storing for each position of the sample the LIBS spectrum. Data processing can then build monochromatic images of the sample at any wavelength by retrieving from the computer memory the proper spectroscopic information for each location.

The LIBS spectrum from the surface of a silicon photovoltaic cell is shown in Figure 1. Single-shot plasma emission on a cell zone located in the interphase between a silver finger and the Ti coating is shown. The crater formed has an elliptical form with approximate surface area of 0.03 mm^2 (see below). Several possible spectral windows were evaluated in order to obtain simultaneous spectral information from the element constituents of the surface and the appropriate signal-to-noise ratio (SNR). The spectral region covering the range 542−657 nm shown in Figure 1 contains peaks corresponding to the sample constituents while providing suitable spectral quality. The peak at 626.168 nm corresponds to Ti(I), that at 546.429 nm to Ag(I), and that at 589.106 nm to C(I) from graphitic carbon present on the sample surface as an impurity. No peaks corresponding to silicon appear as the depth penetration of the laser pulse is lower than the thickness of the TiO_2 coating. In LIBS, line emission is often superimposed on an unspecific background signal due to electron−ion recombination and bremmstrahlung processes. Although the spectrum in Figure 1 shows one of the problems of LIBS, i.e., the lines are broad and may be self-absorbed, in the spectral window chosen, background emission is particularly weak compared to spectral regions at ∼400 nm where other candidate lines for Ti detection are available. Nevertheless, signal and background emission intensity are dependent on the laser irradiance used. Figure 2 shows the Ti signal-to-background ratio (SBR) observed vs the laser irradiance. The Ti line was monitored at 626.168 nm, while the background was measured at 627.3 nm. The laser irradiance was modified by changing the focusing lens to sample distance (working distance, wd). The *x*-axis coordinate in Figure 2 at which the laser is focused at the surface is taken as zero (wd = 0). Negative values of wd refer to the beam focal position placed inside the material, while positive values of wd refer to the beam focused at a distance above the sample surface. No gas breakdown is observed when the laser is focused in front of the sample. The SBR is maximum at the largest irradiance used. However, the signal is not symmetrical at both sides of the wd = 0 coordinate. For identical irradiance at the surface, for instance at wd values of +1 and −1, the SBR is larger for the beam focused inside the sample (wd = −1). Since ablation occurs along the laser propagation direction at both sides of the focal position, a larger amount of material is ablated under these circumstances. However, for the laser focused outside the sample surface, ablation only occurs at one side of the focal position, resulting in lower SBR values.

An important aspect of LIBS imaging is the relationship between spatial resolution and spectral detection. Rigorously speaking, surface information refers to the first layer of atoms on the surface. From this standpoint, LIBS is by far not able to produce truly surface data. Craters of variable depth are formed during single-shot laser ablation, depending on the irradiance used. Since spectral imaging is derived from the crater formed at each sample location, it is of interest to know the range of depth information provided by LIBS. At the irradiance that optimizes the SBR (1.7×10^8 W cm^{-2}, Figure 2), the layer thickness ablated is calculated to be 13 nm. The thickness of the ablated layer was measured using a procedure previously described.[22] The thickness was determined from the number of laser shots needed to deplete completely a film of known thickness (measured by ellipsometry) using a given laser irradiance. For a 40 nm thick layer, four laser shots at 1.7×10^8 W cm^{-2} are needed. It should be noted that the accuracy of this method is limited since the fourth laser shot can ablate a zone containing no TiO_2 in addition to a zone containing TiO_2. Consequently, the ablated depth can be in the range 10−13 nm per pulse. This value should be considered only approximate as the surface morphology of textured silicon makes difficult an accurate determination. The value given provides, however, a typical value of the thickness involved.

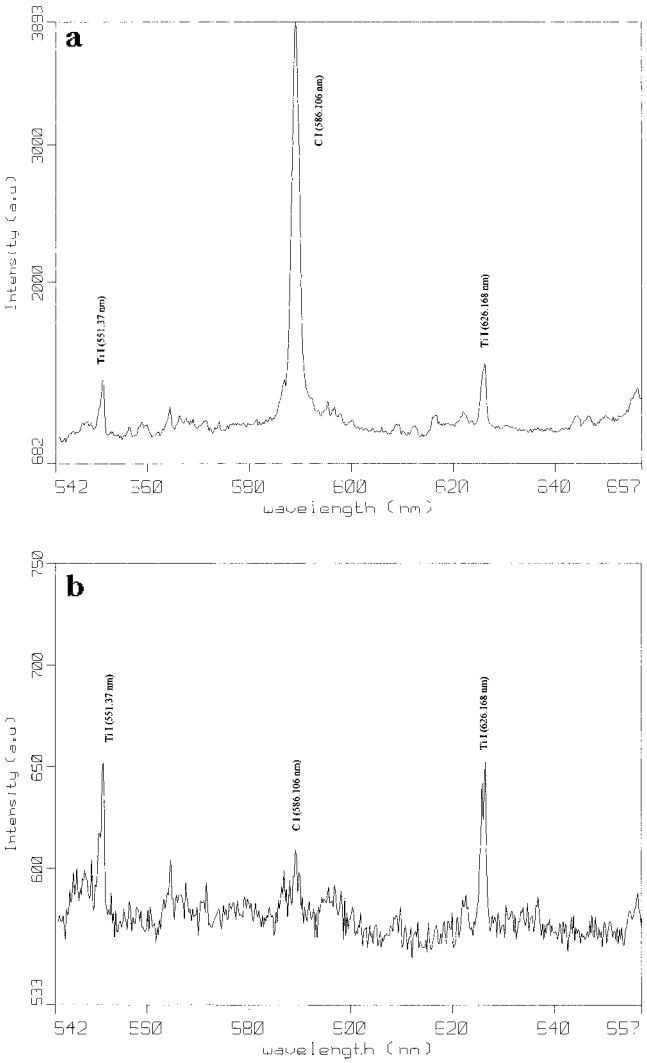

Figure 3. Single-pulse LIBS spectra from a silicon photovoltaic cell surface in a zone between silver fingers obtained at a laser irradiance of (a) 1.7×10^8 and (b) 5×10^7 W cm^{-2}.

Depth resolution can be improved by reducing the laser irradiance. However, this will be done at the expense of the spectral SNR. Figure 3 shows two LIBS spectra obtained at laser irradiances of 1.7×10^8 (Figure 3a) and 5×10^7 W cm^{-2} from a cell zone between silver fingers. At lower irradiance, the thickness ablated is estimated to be ~5 nm. However, the SNR of the associated spectrum is much poorer than that at higher irradiance with 13 nm thickness involved. While the decrease in SNR can be acceptable for imaging major components as in the case of Ti in photovoltaic cells, detection of impurities can be compromised at better depth resolution (lower irradiances), making low-impurity contents undetectable. Figure 3b shows that detection of C will be compromised at 5×10^7 W cm^{-2}. Thus the ultimate limitation to imaging the first layer of the surface in LIBS is the SNR. Even for major components, the ablation threshold limits the minimum irradiance used providing useful spectral information. In this case, it is 4×10^7 W cm^{-2}.

Boundaries are examined in LIBS by orienting them perpendicular to the direction of surface motion and then analyzing a series of points at intervals across the boundary, producing a composition profile. The spacing of the points is selected by considering the extent of the compositional variation and the spatial resolution of the analysis. A useful definition of spatial

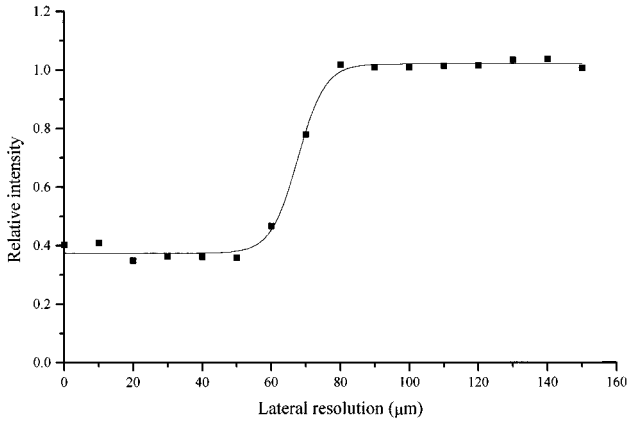

Figure 4. Ratio of peak intensities of the Ti line measured at 626.128 nm from two adjacent points on the surface separated by the distances given in the abscissa axis.

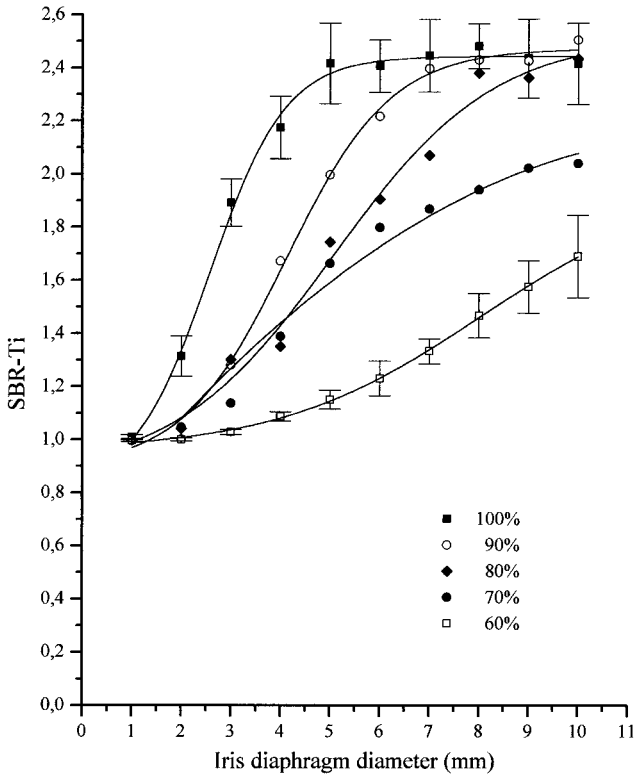

Figure 5. Titanium SBR vs beam diameter for several laser pulse energies. The 100% value (■) corresponds to a nominal pulse energy of 2.5 mJ. Pulse energy was decreased using successive glass plates in the beam path. Bars correspond to the range of 10 measurements.

resolution is provided by the diameter of the beam waist, d, which for a Gaussian laser beam is given by $d = 8\lambda f(\pi D)^{-1}$, where λ is the laser wavelength, f is the focal length of the focusing lens, and D is the diameter of the collimated beam. For the present configuration, using a 4 mm diameter beam and a lens with $f =$ 45 mm, the diffraction-limited beam should be $d \approx 8$ μm. In practice, the crater diameter is much larger than the predicted one due mainly to deviations from the Gaussian distribution, to the thermal conductivity of the surface, and to sputtering of the ablated material. The crater formed on the photovoltaic cell surface at wd = 0 has an elliptical form, with 150 and 70 μm for the larger and shorter dimensions, respectively. The actual lateral resolution with this sample can be accurately determined by measuring the ratio of intensities of Ti peaks measured at the same wavelength from two adjacent points on the surface. Figure

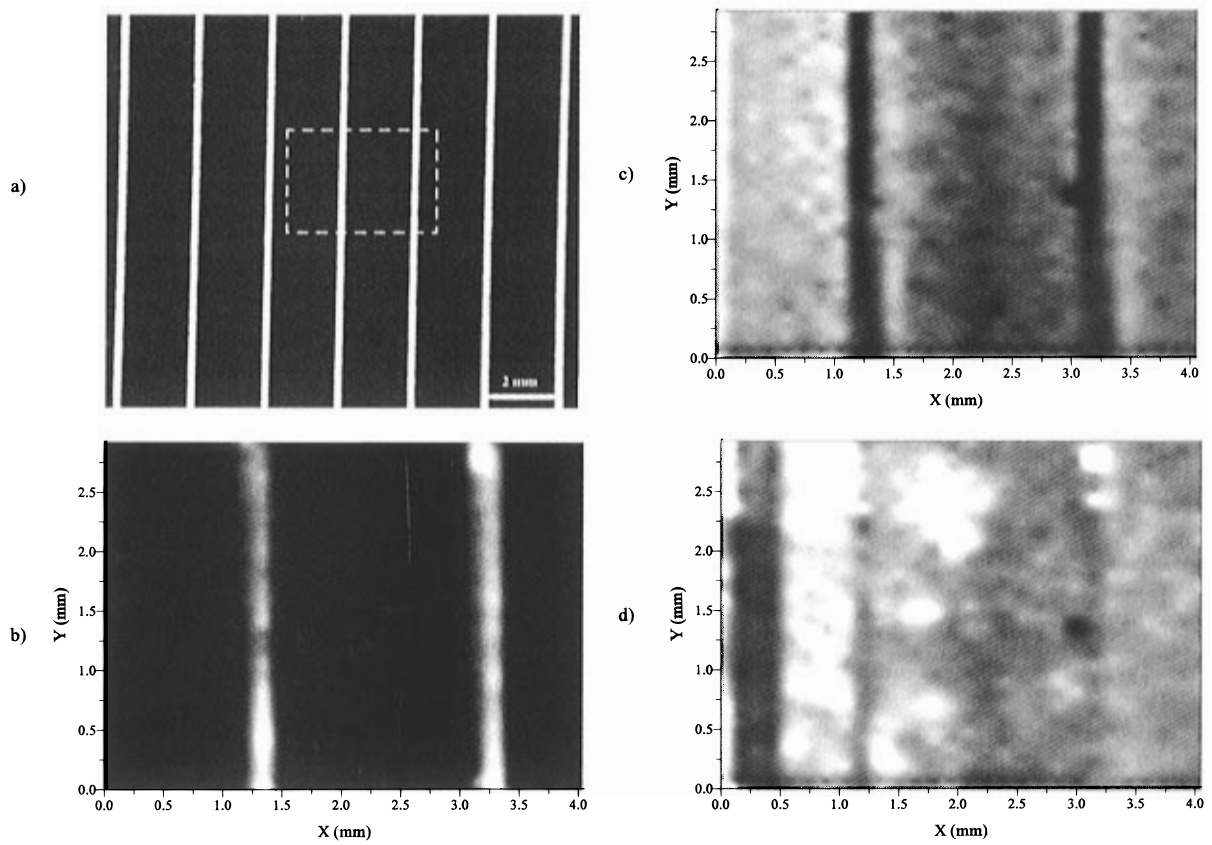

Figure 6. (a) Photomicrograph of a silicon photovoltaic cell. White areas correspond to silver fingers and the black area, to the TiO_2 coating. The zone inside the dotted white line corresponds to the area imaged by LIBS. (b) LIBS image of the spatial distribution of silver (reconstructed from the Ag I line at 546.429 nm). (c) LIBS image of the spatial distribution of Ti (reconstructed from the Ti I line at 626.128 nm). (d) LIBS image of the spatial distribution of carbon (reconstructed from the C I line at 589.106 nm). Single-shot plasma emission from the first laser pulse on the surface was used. The light areas correspond to high elemental contents, and the dark areas correspond to low elemental contents. Laser irradiance 1.7×10^8 W/cm^2. The lateral resolution in the *x* axis was 80 μm.

4 shows the results at increments from 0 to 150 μm in 10 μm steps. As shown, for increments below 60 μm, the ratio of peak intensities is ~0.4, indicating overlapping spots on the surface. At increments over 80 μm, the ratio is close to unity, which means that a new surface is ablated in both cases. Thus the practical spatial resolution is in this case 80 μm. Increasing the laser irradiance with a tightly focused beam results in a larger contribution of depth information and an increased sputtering of material. Data in Figure 4 have been obtained at 1.7×10^8 W cm^{-2}. It should be noted that depth resolution is optimized by defocusing the laser beam or by using low laser irradiance, while for high lateral resolution a tightly focused beam should be used. Therefore, conditions for optimizing lateral resolution can be different from those for optimizing depth resolution.

Another significant aspect of LIBS imaging is the relationship between the surface area sampled, the thickness of the specimen examined, and the laser pulse energy. Figure 5 shows the effect of beam diameter on the Ti SBR for several pulse energies. Data represent averages of 10 laser shots each on fresh surfaces. The SBR increases as the beam diameter increases. However, the SBR does not improve at beam diameters larger than 8 mm for pulse energies of 80% and above. This is because the TiO_2 layer is completely depleted with a single laser shot. The LIBS signal is proportional to the volume of specimen being ablated. For thin specimens, this volume is given roughly by the area of the beam spot multiplied by the specimen thickness. Thus, enlarging the beam diameter is of no sense when the thickness of the layer

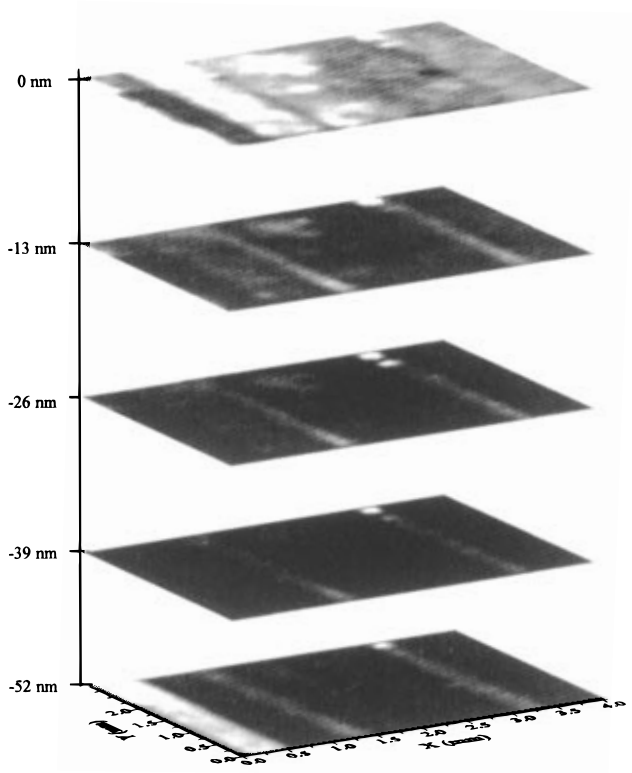

Figure 7. LIBS images of the spatial distribution of carbon (C I line at 598.106 nm) at several depths reconstructed from five consecutive laser shots. Other conditions as in Figure 6.

imaged has been completely ablated by a single laser shot. It produces no improvement in sensitivity, while deteriorating the lateral resolution.

LIBS Images. Figure 6 shows a series of LIBS images at the emission lines of 546.429 nm, 626.168 nm , and 589.106 nm, indicating the spatial distribution of Ag, Ti, and C, respectively, on the surface of the photovoltaic cell. For comparison purposes, a photomicrograph showing the imaged surface area is also presented (Figure 6a). In this figure the white areas correspond to silver fingers and the black area, to the TiO_2 coating. The LIBS images were reconstructed from single-shot plasma emission using the first laser pulse. The images display the expected features without distortion; both the silver fingers and the TiO_2 areas are well defined. Carbon shows an irregularly spaced distribution, appearing both on the silver fingers and on the TiO_2 coating. The spatial resolution of the images is 80 μm in the direction perpendicular to the silver fingers. The depth resolution is $\sim$13 nm in the zones between silver fingers.

Figure 7 shows the images of carbon distribution obtained from five consecutive laser shots. Carbon content between silver fingers decreases steadily with depth up to 39 nm, while it remains virtually constant in the silver fingers. However, at a depth of 52 nm, the carbon distribution between fingers changes suddenly (see the bottom left zone). This is because the TiO_2 coating has been completely removed and the silicon substrate has been reached. Since the silver fingers penetrate into the silicon, the carbon content in the fingers remains unchanged at a depth of 60 nm.

In the present configuration, the imaging time is limited by the spatial resolution and by the reading time of the CCD. For improved spatial resolution, an increased imaging time is necessary. This time can be reduced by increasing the laser repetition rate. In this paper, images based on single-shot laser plasmas were acquired at 2 Hz, which results in a data acquisition time of 5 min for imaging a 4.5×3 mm^2 area at spatial resolution of 80 μm.

CONCLUSIONS

Multielemental chemical imaging using laser-induced breakdown spectrometry is an effective method for simultaneous distribution analysis of solid surfaces. Both surface and depth distributions are amenable with this approach. The use of laser irradiances below the air breakdown allows working at atmospheric pressure without spectral interference from air elements. In addition, the capability of imaging conductive and insulating materials offers clear advantages for imaging samples of variable size. This approach is therefore potentially applicable to a wide range of elements and surfaces. Although LIBS is a typical example of destructive analytical technique, multichannel detection as demonstrated here confers the possibility to LIBS of obtaining multielement information from a given surface area. With the present configuration, the lateral resolution is 80 μm and the depth resolution is $\sim$13 nm for TiO_2 coatings. Using highly coherent laser beams and refined optical elements, in-plane resolution could be substantially improved. Enhanced depth resolution is more difficult to attain, and possibly improvements can be achieved by increasing significantly the angle of incidence of the laser beam on the sample surface. In both cases, the main limiting factor to resolution is the ablation threshold of the material.

Received March 20, 1997. Accepted May 16, 1997.[⊗]

AC9703111

[⊗] Abstract published in *Advance ACS Abstracts,* July 1, 1997.